

# Percolative analysis of 3D vasculogenesis

F. Cavalli<sup>1</sup>, A. Gamba<sup>2</sup>, G. Naldi<sup>1</sup>, M. Semplice<sup>1</sup>, and G. Serini<sup>3</sup>

<sup>1</sup> Dipartimento di Matematica, Università degli Studi di Milano, via Saldini 50, 20133 Milano, Italia. [cavalli,naldi,semplice@mat.unimi.it](mailto:cavalli,naldi,semplice@mat.unimi.it)

<sup>2</sup> Dipartimento di Matematica, Politecnico di Torino, Corso Duca degli Abruzzi 24, 10129, Torino, and INFN, unità di Torino, via P. Giuria 1, 10125 Torino, Italia. [andrea.gamba@polito.it](mailto:andrea.gamba@polito.it)

<sup>3</sup> Department of Oncological Sciences and Division of Molecular Angiogenesis, Institute for Cancer Research and Treatment, University of Torino School of Medicine, Strada Provinciale 142 Km 3.95, 10060 Candiolo (TO), Italia. [guido.serini@ircrc.it](mailto:guido.serini@ircrc.it)

**Abstract** Vascular networks form by the spontaneous aggregation of individual cells migrating toward vascularization sites (vasculogenesis). The study of this fascinating process is performed by biologists using *in vitro* and *in vivo* assays, both in twodimensional and threedimensional settings. A succesfull theoretical model of twodimensional experimental vasculogenesis has been recently proposed, showing the relevance of percolation concepts and of cell cross-talk (chemotactic autocrine loop) to the understanding of the self-aggregation process. Here we study the natural 3D extension of the earlier proposed computational model, which we take as a starting point for the investigation of the genuinely threedimensional process of vasculogenesis in vertebrate embryos. The computational model is based on a multidimensional Burgers equation, which is a well studied paradigm in the research on spontaneous pattern formation, integrated with a feedback term describing the chemotactic autocrine loop. The numerical approximation of the computational model poses several technical problems which are here briefly discussed. Starting from initial conditions mimicking the experimentally observed ones the numerical simulations produce network-like structures qualitatively similar to those observed in the early stages of *in vivo* vasculogenesis. Following the lesson learned in the twodimensional case, we develop the computation of critical percolative indices as a robust measure of the network geometry.

## 1 Introduction

In recent years, biologists have collected many qualitative and quantitative data on the behavior of microscopic components of living beings. We are, however, still far from understanding how these microscopic components interact to build functions which are essential for life. A problem of particular interest is the formation of patterns through various types of simmetry breaking of initially homogeneous systems. Such patterns often show self-similarity and scaling laws [15] similar to those emerging in the physics of phase transitions [21].

The vascular network [24, 25] is a typical example of natural structure characterized by non trivial scaling laws. In recent years many experimental investigations have been performed on the mechanism of blood vessel formation [3] both in living beings and in *in vitro* experiments.

Vascular networks form by the spontaneous aggregation of individual cells travelling toward vascularization sites (vasculogenesis). Today, the vascularization process is observable in real time thanks to the progress in imaging technologies.

The questions that naturally come to mind when observing this kind of morphogenetic process are: by which mechanism the dynamics of separate individuals can be coordinated to build up sophisticated tissue structures, as if following an invisible blueprint? where is the blueprint of the structure really encoded?

An answer to this kind of questions comes from theoretical modelling. One can develop computational models based on simple dynamical principles and test whether they are able to reproduce the experimentally observed features. If the basic dynamical principles are correctly chosen, computational experiments allow to observe the emergence of complex structures from a multiplicity of interactions following simple rules.

Apart from the purely theoretical interest, reproducing biological dynamics by computational models allows to identify those biochemical and biophysical parameters which are mainly driving the process. This way, computational models can produce a deeper understanding of biological mechanisms, which in principle may end up having relevant practical consequences.

This path was followed in the study of twodimensional experimental vasculogenesis. By theoretical modelling it was shown that the formation of the experimentally observed structures can be explained as the consequences of cell motility and of cell cross-talk mediated by the exchange of soluble chemical factors (chemotactic autocrine loop). The model also shows that the main factors determining the qualitative properties of the observed vascular structures are the available cell density and the diffusivity and half-life of the soluble chemical exchanged.

The mysterious blueprint does not really exists: what is actually encoded in the genes are the dynamical rules followed by the individual cell. The interplay of these simple dynamical rules with the geometrical and physical properties of the environment produces the highly structured final result. One is tempted to speculate that organized tissue structures such as vascular networks have actually evolved out of preexisting (chemotactic, migrating) forms of behavior of simple cells.

At the moment, no direct observation of the chemotactic autocrine loop regulating vascular network formation is available, although several indirect biochemical observations point to it, so, the main evidence in this sense still comes from experimental and theoretical analysis of computational models.

Comparison of experimental observations to computational models must be quantitative and based on the measurement of robust geometrical features. Moreover, observable quantitities must have a principally statistical meaning, to over-

come the obvious difficultly presented by the large variability of the properties of observed samples. A lesson to this regard comes from the study of twodimensional vasculogenesis, where experimental assays are realized by scattering a controlled cell density  $n$  on an appropriate gel surface. By varying the cell density  $n$  one observes a percolative transition.

Percolation is defined as the formation of connected cell clusters extending between opposite sites of the system boundary, thus allowing the transport of blood in the living system. The transition consists in the fact that for low cell densities percolating clusters do not exist, while they start appearing at a well-defined critical density  $n_c$ . An interesting fact is that in the vicinity of the critical density  $n_c$  the geometric properties of clusters show a peculiar scaling behavior. For instance, the probability of percolation  $\Pi(n, L)$ , defined empirically as the fraction of computational experiments that produce a percolating cluster, is actually a function of the combination  $(n - n_c) L^{1/\nu}$ , where  $\nu$  is a universal exponent. Universal exponents such as  $\nu$  are known to be functions of the type of aggregation dynamics observed, whose value does not change when varying dynamical parameters in large regions of the parameter space. We have thus two reasons to study percolation in relation to vascular network formation: (i) percolation is a fundamental property for vascular networks: blood should have the possibility to travel through the whole vascular network to carry nutrients to tissues; (ii) critical exponents are robust observables characterizing the aggregation dynamics.

Up to now, the comparison of the computational model with experimental observations has been successful but limited to twodimensional settings. This is related to the fact that most experiments in experimental vasculogenesis are actually realized by seeding cells on a twodimensional gel matrix. However, it is obvious that a complete understanding of the vascularization process is possible only if it is considered in its natural threedimensional setting ([1, 4]).

In the embryo, endothelial cells are produced and migrate in a sort of threedimensional scaffold, the extracellular matrix. Migration is actually performed through a series of biochemical processes, such as sensing of chemotactic gradients, and of mechanical operations, such as extensions, contractions, and breaking of the extracellular matrix along the way.

Evidence have been provided in twodimensional experimental vasculogenesis that cell motion is directed by an autocrine loop of soluble chemoattractant factors. Since cells are usually living in 3D, it is natural to suppose that this kind of directed motion is still playing a relevant role in the natural threedimensional environment.

Several major developments in cell and tissue imaging allow today to observe in real time the mechanisms of cell migration and aggregation in threedimensional settings. This is due to progress in microscopy techniques and in image analysis software, including tracking tools to monitor the position of cells and particles in real time [6].

Multicellular aggregates or tissue explants can be integrated into 3D extracellular matrix, such as a 3D collagen lattice or thick reconstituted basement membrane (matrigel).

*In vivo* experiments in a genuine 3D setting can be done in transparent tissues, such as those of the chick embryo.

In this paper we give preliminary result on the investigation of vascular network formation in an *in vivo* threedimensional environment both from an experimental and a theoretical point of view.

From the experimental point of view, we present images of vascular network formation in chick embryo at different stages of development, obtained by confocal microscopy. At an early stage of development one observes immature vascular networks formed by vasculogenesis. At subsequent stages one observes initial remodelling, which becomes more evident at later stages, where blood vessels become organized in a mature and hierarchically organized vascular network.

From the theoretical viewpoint, we consider the natural threedimensional extension of the model proposed in Refs. [7, 19]. The model is based on a Burgers-like equation, a well studied paradigm in the theory of pattern formation, integrated with a feedback term describing the chemotactic autocrine loop.

The numerical evolution of the computational model starting from initial conditions mimicking the experimentally observed ones produces network-like structures qualitatively similar to those observed in the early stages of *in vivo* vasculogenesis.

Since in the long run we are interested in developing quantitative comparison between experimental data and theoretical model, we start by selecting a set of observable quantitatis which provide robust quantitative information on the network geometry. The lesson learned from the study of twodimensional vasculogenesis is that percolative exponents are an interesting set of such observables, so we test the computation of percolative exponents on simulated network structures.

A quantitative comparison of the geometrical properties of experimental and computational network structure will become possible as soon as an adequate amount of experimental data, allowing proper statistical computation, will become available.

The paper is organized as follows. Section 2 summarizes some background knowledge on the biological problem of vascular network formation and contains a description of the experimental observations. Section 3 is a short review of the properties of the model introduced in [7, 19]. In Section 4 the numerical approximation technique for this model is described. In Section 5 we describe the qualitative properties of the simulated network structures. In Section 6 we present the results of the computation of the exponents of the percolative transition. Finally, in the Conclusions, we point out at predictable developments of our research.

## 2 Biological framework and experimental observations

To supply tissues with nutrients in an optimal way, vertebrates have developed a hierarchical vascular system which terminates in a network of size-invariant units, *i.e.* capillaries. Capillary networks characterized by intercapillary distances ranging from 50 to 300  $\mu\text{m}$  are essential for optimal metabolic exchange [8].

Capillaries are made of endothelial cells. Their growth is essentially driven by two processes: vasculogenesis and angiogenesis [3]. Vasculogenesis consists of local differentiation of some precursor cells to endothelial ones, that assemble into a vascular network by directed migration and cohesion. Angiogenesis is, essentially, characterized by sprouting of an immature structure and remodeling.

In twodimensional assays, the process of formation of a vascular network starting from randomly seeded cells can be accurately tracked by videomicroscopy [7] and it is observed to proceed along three main stages: *i*) migration and early network formation, *ii*) network remodeling and *iii*) differentiation in tubular structures. During the first phase, which is the most important for the final geometrical properties of the structures, cells migrate over distances which are an order of magnitude larger than their radius and aggregate when they get in touch with one of their neighbors. Their dynamics is well reproduced by the theoretical model proposed in Ref. [7].

An accurate statistics of individual cells trajectories has been presented in Ref. [7], showing that in the first phase cell motion has marked persistence in the initial direction, pointing toward zones of higher concentrations of cells. This indicates that cells communicate among them through the emission of soluble chemical factors that diffuse and degrade in the surrounding medium, and suggests that they move toward the gradients of this chemical field. Cells behave like not-directly interacting particles, the interaction being mediated by the release of chemotactic factors.

It is extremely likely that the chemotactic autocrine loop observed in twodimensional vasculogenesis is also at work in real threedimensional vasculogenesis.

Observation of *in vitro* vasculogenesis can be performed in transparent tissues, such as chick embryo, with a confocal microscope.

We provide here  $(750 \mu\text{m})^2$  images of chick embryo brain at different development stages (Fig. 1). Embryo development stages are usually classified according to Hamilton and Hamburger (HH classification). Wheat germ agglutinin (WGA) marked with the fluorescent traces Alexa-488 was injected in embryos. The embryos were fixed in paraphormaldeid and the brain analyzed with a 20x objective using a 488 nm light generated by an Argon laser. Observed development stages were HH stages 17, 20 and 26. At the early stage HH17 one observes a typical immature vascular network formed by vasculogenesis and characterized by a high density of similar blood vessels (Fig. 1A). At the HH20 stage we observe initial remodeling of the vascular network (Figs. 1B,C). Remodeling becomes more evident at stage HH26 where blood vessels are organized in a mature, hierarchically organized vascular tree (Fig. 1D).

Images have been collected as a series of  $1024 \times 1024$  pictures representing sections taken at distances varying from 4 to 10  $\mu\text{m}$ . A Free Maximum Projection

has been constructed by the microscope software by superimposing the different sections and assigning higher luminosity intensities to higher standing sections, thus obtaining a pseudo 3D image giving an overall idea of the imaged sample.

Images corresponding to the different sections will be in the next future reconstructed to provide 3D models to be compared with the results of numerical simulations of the theoretical model.

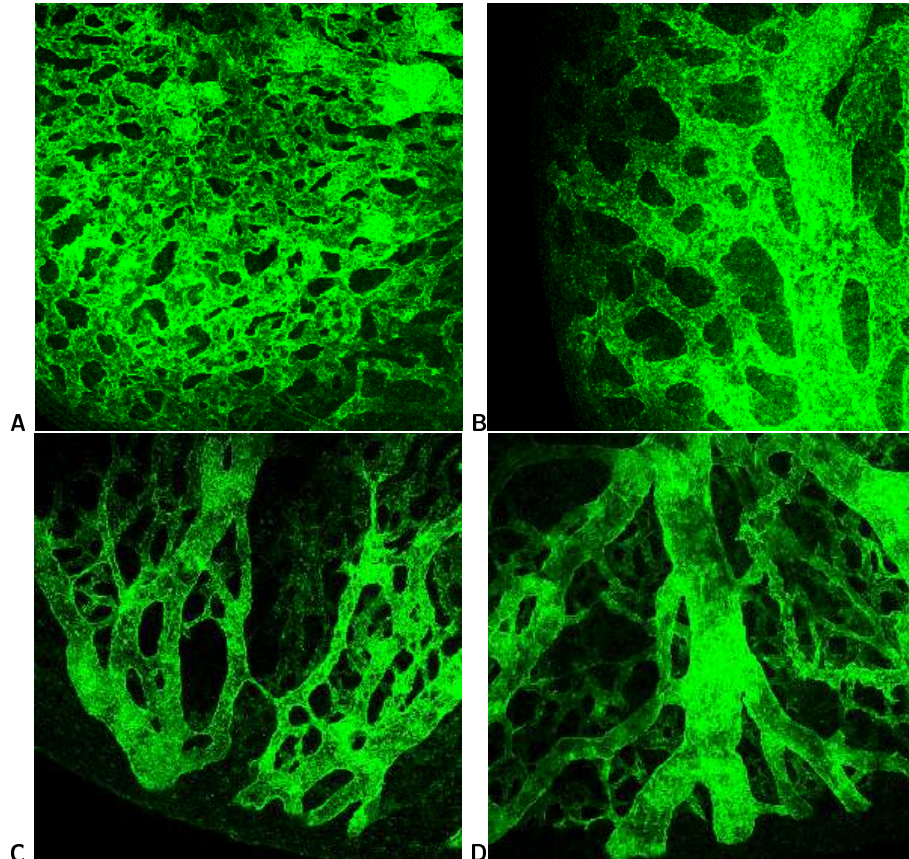


**Figure1.** Vascular networks formed by vasculogenesis in chick embryo brain, at variuos stages of development, classified according to Hamilton and Hamburger (HH). **A:** HH stage 17; **B:** HH stage 20; **C:** HH stage 26; **D:** HH stage 26.

### 3 Computational model

The multidimensional Burgers' equation is a well-known paradigm in the study of pattern formation. It gives a coarse grained hydrodynamic description of the mo-

tion of independent agents performing rectilinear motion and interacting only at very short ranges. These equations have been utilized to describe the emergence of structured patterns in many different physical settings [20, 12]. A particular interesting system is that of weakly interacting sticky matter. In the early stages of dynamics, each particle moves with a constant velocity, given by a random statistical distribution. This motion gives rise to intersection of trajectories and formation of shock waves. After the birth of these local singularities regions of high density grow and form a peculiar network-like structure. The main feature of this structure is the existence of comparatively thin layers and filaments of high density that separate large regions of low density. The behavior of these systems can be described in detail by Burgers' equation [2]:

$$\frac{\partial \mathbf{v}}{\partial t} + \mathbf{v} \cdot \nabla \mathbf{v} = \nu \nabla^2 \mathbf{v} \quad (1)$$

coupled with the mass-conservation law:

$$\frac{\partial n}{\partial t} + \nabla \cdot (n \mathbf{v}) = 0 \quad (2)$$

The arbitrary parameter  $\nu$  can be interpreted as viscosity, even if the way it enters into the equation implies a model description of viscosity rather than a physical one.

In order to study and identify the factors influencing blood vessel formation, one has to take into account evidence suggesting that cells do not behave as independent agents, but rather exchange information in the form of soluble chemical factors. This leads to the model proposed in Gamba et al. in [7] and by Serini et al. in [19]. The model describes the motion of a fluid of randomly seeded independent particles which communicate through emission and absorption of a soluble factor and move toward its concentration gradients, and allows to well reproduce both the observed percolative transition and the typical scale of twodimensional vascular networks.

In the model, the cell population is described by a continuous density  $n(\mathbf{x}, t)$ , where  $\mathbf{x} \in \mathbf{R}^d$  ( $d = 2, 3$ ) is the space variable, and  $t \geq 0$  is the time variable. The population density moves with velocities  $\mathbf{v}(\mathbf{x}, t)$ , that are triggered either by chemical gradients of a soluble factor or by random motion. The chemoattractant is described by a scalar chemical concentration field  $c(\mathbf{x}, t)$ . Moreover, the chemical factor is supposed to be released by the cells themselves, diffuse, and degrade in finite time, in agreement with experimental observations. These assumptions give rise to the following system:

$$\frac{\partial n}{\partial t} + \nabla \cdot (n \mathbf{v}) = 0 \quad (3a)$$

$$\frac{\partial \mathbf{v}}{\partial t} + \mathbf{v} \cdot \nabla \mathbf{v} = \mu(c) \nabla c - \nabla \phi(n) - \beta(c) \mathbf{v} \quad (3b)$$

$$\frac{\partial c}{\partial t} = D \Delta c + \alpha(c) n - \frac{c}{\tau} \quad (3c)$$

Here  $\mu$  measures the cell response to the chemotactic factor, while  $D$  and  $\tau$  are respectively the diffusion coefficient and the characteristic degradation time of the soluble chemoattractant. Finally the function  $\alpha$  determines the rate of release of the chemical factor. The friction term  $-\beta\mathbf{v}$  mimics the adhesion of the cells to the extracellular matrix.

A simple model may be obtained by assuming that the cell sensitivity  $\mu$ , the rate of release of the chemoattractant  $\alpha$  and the friction coefficient  $\beta$  are constant. A more realistic description may be obtained including saturation effects as dependences on the concentration  $c$  of the aforementioned coefficients.

The term  $\nabla\phi(n)$  is a density dependent pressure term where  $\phi(n)$  is zero for low densities, and increases for densities above a suitable threshold. This pressure is a phenomenological term which models short range interaction between cells and the fact that cells do not penetrate and have some degree of rigidity.

The meaning of the model equations is the following. Eq. (3) expresses the conservation of the number of cells. At low densities, (3) is an inviscid Burgers' equation for the velocity field  $\mathbf{v}$  [2], coupled to the standard reaction-diffusion equation (3). In Burgers' equation matter in the earlier stages of its evolution is described as a fluid of free, non-interacting particles. After a characteristic time, faster particles catch up the slower ones and form a network of shock waves, which in two dimensions are strikingly similar to capillary-like networks.

Fourier analysis of Eq. (3) in the fast diffusion approximation ( $\partial c/\partial t = 0$ ) suggests that starting from the above mentioned initial conditions, Eq. (3) should develop network patterns characterized by a typical length scale  $r_0 = \sqrt{D\tau}$ , which is the effective range of the interaction mediated by soluble factors. As a matter of fact, Fourier components  $c_k$  are related to the Fourier components of the density field  $n_k$  by the relation  $c_k = \frac{\alpha\tau n_k}{D\tau k^2 + 1}$ . This means that in Eq. (3) wavelengths of the field  $n$  of order  $r_0$  are amplified, while wavelengths  $\lambda \gg r_0$  or  $\lambda \ll r_0$  are suppressed.

Initial conditions introduce in the problem a typical length scale given by the average cell-cell distance  $L/\sqrt{N}$ , where  $L$  is the system size and  $N$  the particle number. The dynamics, filtering wavelengths [5], rearranges matter and forms a network characterized by the typical length scale  $r_0$ .

It is interesting to check the compatibility of the theoretical prediction with physical data. From available experimental results on two-dimensional plates [17] it is known that the order of magnitude of the diffusion coefficient for major angiogenic growth factors is  $D = 10^{-7} \text{ cm}^2 \text{ s}^{-1}$ . In the experimental conditions that were considered the half time of soluble factors is  $64 \pm 7 \text{ min}$  [7]. This gives  $r_0 \sim 200 \mu\text{m}$ , a value in good agreement with experimental observations.

Since in the early stages of development almost all intraembryonic mesodermal tissues contain migrating endothelial precursors, which appear to be randomly scattered, we use initial conditions representing a randomly scattered distribution of cells, *i.e.*, we throw an assigned number of cells in random positions inside the cubic box, with zero initial velocities and zero initial concentration of the soluble factor, with a single cell given initially by a Gaussian

bump of width  $\sigma$  of the order of the average cell radius ( $a \simeq 30\mu\text{m}$ ) and unitary weight in the integrated cell density field  $n$ .

## 4 Numerical methods

In order to write a reliable numerical scheme to integrate system (3), we need to rewrite the first and second equation in conservative form. Introducing the moment  $\mathbf{p}(\mathbf{x}, t) = n(\mathbf{x}, t)\mathbf{v}(\mathbf{x}, t)$ , the system may be recast in the following form:

$$\frac{\partial n}{\partial t} + \nabla \cdot \mathbf{p} = 0 \quad (4a)$$

$$\frac{\partial \mathbf{p}}{\partial t} + \nabla \left( \frac{\mathbf{p}^2}{n} \right) = n\mu \nabla c - n\nabla\phi(n) - \beta\mathbf{p} \quad (4b)$$

$$\frac{\partial c}{\partial t} = D\Delta c + \alpha n - \frac{c}{\tau} \quad (4c)$$

We introduce a regular grid in the computational domain with space step  $dx$  and time step  $dt$  and use finite differences. We approximate the continuous variables  $n, \mathbf{p}, c$  with their values  $n_{i,j,k}, \mathbf{p}_{i,j,k}, c_{i,j,k}$  at the centre of each computational cell indexed by the triple  $(i, j, k)$ .

Equation (4) is linear hyperbolic and may be integrated by choosing an appropriate numerical flux to approximate the advection operator. The use of slope limiters in the flux ([14]) in combination with a forward Euler time integrator gives a non-oscillatory numerical scheme that is second order accurate.

Similarly, equation (4) may be treated by approximating the Laplacian with the usual finite difference formula with on a stencil with three points in each direction. Explicit Euler integration requires a restriction of type  $dt < C(dx)^2$  on the time step.

The second equation, however, is non-linear hyperbolic and we wish to avoid the use of Riemann solvers and to avoid recomputing the characteristic structure at each time step. In order to achieve this, we replace it with a relaxation system of two semi-linear equations with stiff source terms. The transport operator is now linear and its characteristic structure is constant both in time and for every cell. Hence solving these two equations with an IMEX scheme that combines implicit time integration for the stiff terms and an explicit method for the non stiff transport operator is now feasible. Moreover this gives rise to an algorithm with very good scaling properties on parallel computers.

Starting from a general scalar conservation law with source term

$$\frac{\partial u}{\partial t} + \frac{\partial}{\partial x} f(u) = g(u), \quad (5)$$

Jin and Xin [11] have proposed the following relaxation system

$$\frac{\partial u}{\partial t} + \frac{\partial j}{\partial x} = g(u) \quad (6a)$$

$$\frac{\partial j}{\partial t} + a \frac{\partial u}{\partial x} = -\frac{1}{\epsilon}(j - f(u)), \quad (6b)$$

where  $j$  plays the role of a physical flux,  $\epsilon$  is a small positive parameter, called relaxation time, and  $a$  is a suitable positive constant. The first order approximation of the conservation law (6) is

$$\frac{\partial u}{\partial t} + \frac{\partial}{\partial x} f(u) = g(u) + \epsilon \frac{\partial}{\partial x} \left( (a - f'(u)^2) \frac{\partial u}{\partial x} \right), \quad (7)$$

which can be derived using the Chapman-Enskog expansion. It is also clear that (4) is dissipative, provided that the subcharacteristic condition  $a > f'(u)^2$  is satisfied. We would expect that appropriate numerical discretization of the relaxation system (6) yields accurate approximation to the original equation (4) when the relaxation parameter  $\epsilon$  is sufficiently small.

In view of its numerical approximation, the main advantage of the relaxation system (6) over the original equation (4) lies in the linear structure of the characteristic fields and in the localized low order term. In particular this linear structure avoids the use of time consuming Riemann solvers. Moreover, proper implicit time discretizations can be exploited to overcome the stability constraints due to the stiffness and to avoid the use of non-linear solvers.

The so-called relaxed scheme, i.e. the one obtained when  $\epsilon \rightarrow 0$ , reduces to a relaxation step that integrates with the implicit Euler method the system

$$\begin{cases} j = f(u) \\ u_t = g(u) \end{cases}$$

followed by a transport step that integrates with the forward Euler method the system

$$\begin{cases} u_t + j_x = 0 \\ j_t + au_x = 0 \end{cases}$$

This latter step is performed by changing into the characteristic variables  $u \pm j$  to decouple the two equations and choosing numerical fluxes as briefly described for equation (4). Taking into account the form of our function  $f$  and the bound on  $a$ , the restriction on the time step is of the form  $dt < \frac{dx}{\max(v)}$ . For the velocities  $v$  and grid spacing  $dx$  that arise in our simulations, this upper bound of the same order of the one arising from the parabolic condition for equation (4). Clearly, finer grids would require an implicit time integrator for the diffusion equation to avoid severe restrictions on the time step.

In the case of multidimensions, a similar discretization can be applied to each space dimension [11, 10, 16]. Then, since the structure of the multidimensional relaxation system is similar to the 1D system, the numerical implementation for higher dimensional problems, based on additive dimensional splitting, is not much harder than for 1D problems.

## 5 Numerical results

We perform threedimensional numerical simulations of model (3) on a cubic box with side of length  $L = 1\text{mm}$ , with periodic boundary conditions. In particular

equation (3) is solved replacing it with a relaxation system that is solved numerically by considering the splitting scheme for the pure convective step and the relaxation step that was described in the previous section. For the numerical discretization of the transport step, in order to achieve an accuracy of  $O(\Delta x^2)$ , we use a second order total variation diminishing scheme with suitable slope limiter (see [9, 23]).

Biochemical experiments suggest the values of  $D = 10^{-3} \text{ mm}^2/\text{sec}$  and  $\tau = 4000 \text{ s}$  for the diffusion constant and the decay rate of the chemoattractant. We fix the other constant parameters by dimensional analysis and the consideration of the characteristic scales of the system. In particular, we choose:  $\mu_0 = 10^{-11} \text{ mm}^4/\text{sec}^3$ ,  $\alpha = 1 \text{ sec}^{-1}$ ,  $\beta = 10^{-3} \text{ sec}^{-1}$ .

The pressure function is taken to be

$$p(n) = \begin{cases} C_p(n - n_0)^3 & n > n_0 \\ 0 & n \leq n_0 \end{cases}$$

where  $n_0 = 1.0$ .

With this setting, we observe that the initial random distribution of cells evolve into a network that actually represents a transient state.

However, biological observation show that the dynamics of cell changes when they establish cell-cell contacts. It is reasonable to suppose that a different genetic program is activated at this moment, disabling cell motility. We therefore switch off cell motility as soon as the cell concentration, signalled by its chemoattractant emission, reaches a given threshold. This way also the computational system is guaranteed to reach a stationary state.

These effects may be incorporated in our model using a non-constant sensitivity  $\mu(c)$ , a non-linear emission rate  $\alpha(c)$ , or a variable friction coefficient  $\beta(c)$ . We choose a threshold  $c_0$  and then functions like

$$\mu(c) = \mu_0(1 - \tanh(c - c_0)) \quad (8a)$$

$$\alpha(c) = \alpha_0(1 - \tanh(c - c_0)) \quad (8b)$$

$$\beta(c) = \beta_0(1 + \tanh(\gamma(c - c_0)))/3.0 \quad (8c)$$

The net effect is that the sensitivity of the cells and respectively their production of chemoattractant is strongly damped when the concentration  $c$  reaches the threshold  $c_0$ . We did not observe a significant dependence on the exact form of the damping function, provided that it approximates a step function that is nonzero only when  $c < c_0$ .  $\beta(c)$ , on the other hand has the effect of turning on a strong friction term at locations of high concentration of chemoattractant. We performed several tests and observed that these methods are approximately equivalent in freezing the system into a network-like stationary state.

Very fine grids have to be used, in order to resolve the details of the field  $n(\mathbf{x}, t)$ , which might have hundreds of small bumps, each representing a single cell. In order to describe accurately Since each cell has radius  $\sigma = 30 \mu\text{m}$ , one needs a grid spacing such that  $\Delta x < 10 \mu\text{m}$  and this gives rise to grids of at least  $100^3$  cells for a cubic domain of side 1mm.

The computational cost is quite high and may be reduced by using parallel computing: the semilinearity of relaxation systems, together with appropriate discretizations, gives rise to parallel algorithms with almost optimal scaling properties. We implemented the algorithm on a high performance cluster for parallel computation installed at the Department of Mathematics of the University of Milano (see <http://cluster.mat.unimi.it/>). The scaling properties of the algorithm are shown in Figure 5 and are essentially due to the exclusive use of matrix-vectors operations and to the avoidance of solvers for linear or non-linear systems.

Our choice of a numerical algorithm that performs only linear operations and local function evaluations allows us to obtain very good scaling properties in the parallel implementation, as shown in Figure 5.

We observed that, starting with an initial random distribution of cells, the cell density evolves towards a network-like state. We performed numerical simulations with randomly assigned initial cell positions for various cell densities  $\bar{n}$ . We observed a percolative behaviour similar to the one described in [7] for the two-dimensional system. A detailed analysis is given in the following section.

## 6 Analysis of the percolative phase transition

The purely geometric problem of percolation represents one of the simplest phase transition occurring in nature. Many percolative models show a second order phase transition in correspondence to a critical value  $n_c$ , *i.e.* the probability  $\Pi$  of observing an infinite cluster is 0 for  $\bar{n} < n_c$  and 1 for  $\bar{n} > n_c$  [22].

The phase transition can be studied by observing the values of an order parameter, *i.e.* an observable quantity that assumes nonzero values only on one side of the phase transition. In a percolation problem it is natural to chose as order parameter the probability  $P$  that a randomly chosen site belongs to an infinite cluster (on finite grids, the infinite cluster is taken to be the biggest one).

Another interesting observable quantity (analogue to the magnetic susceptibility in a ferromagnetic transition) is the average cluster size

$$S = \frac{\sum_s N_s s^2}{\sum_s N_s s}$$

where  $N_s$  is the number of clusters of size  $s$ , excluding from the sum the infinite cluster.  $S$  is the average size (number of sites) to which a randomly chosen occupied site in the lattice belongs.

The correlation (or connectivity) function  $c(r)$  is defined as the probability that two randomly chosen sites at distance  $r$  are occupied on the same cluster and the correlation (or connectivity) length as

$$\xi^2 = \frac{\sum r^2 c(r)}{\sum c(r)}$$

where the sum is performed over sites.

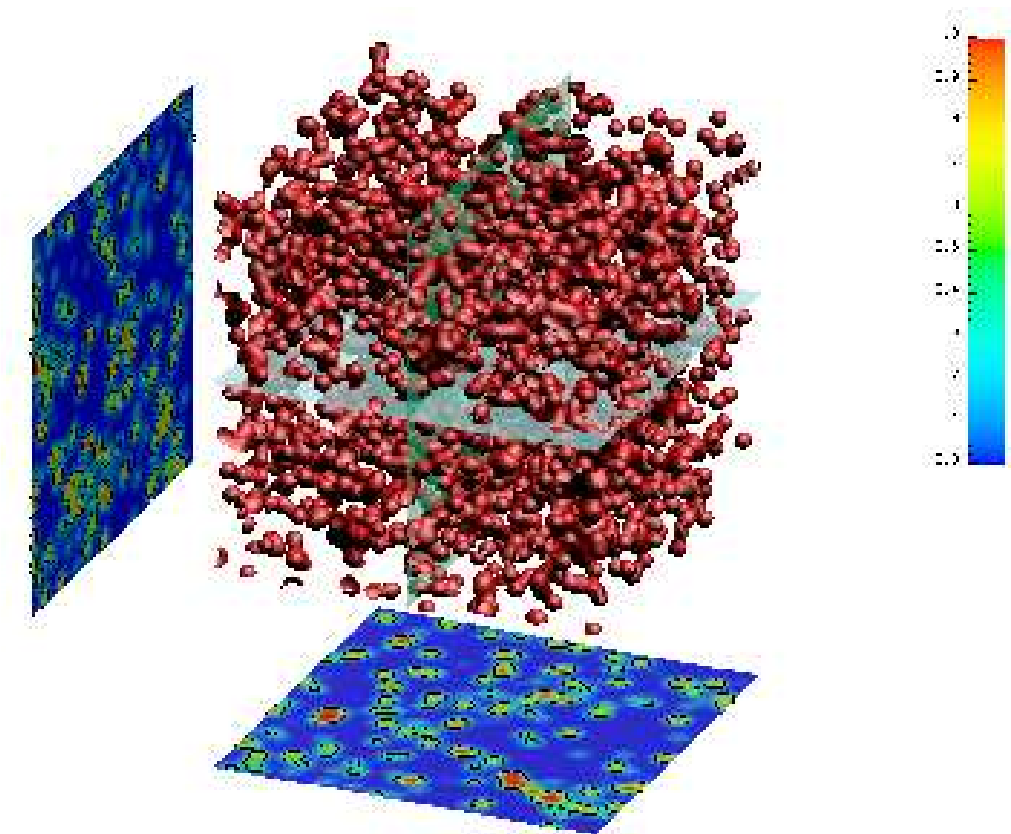


**Figure2.** Plot of the initial state of a numerical simulation with  $2500\text{cells/mm}^3$ . The colorbar on the right is referred to the coloring of the cross sections. The red three-dimensional isosurface corresponds to the black contour lines in the cross sections

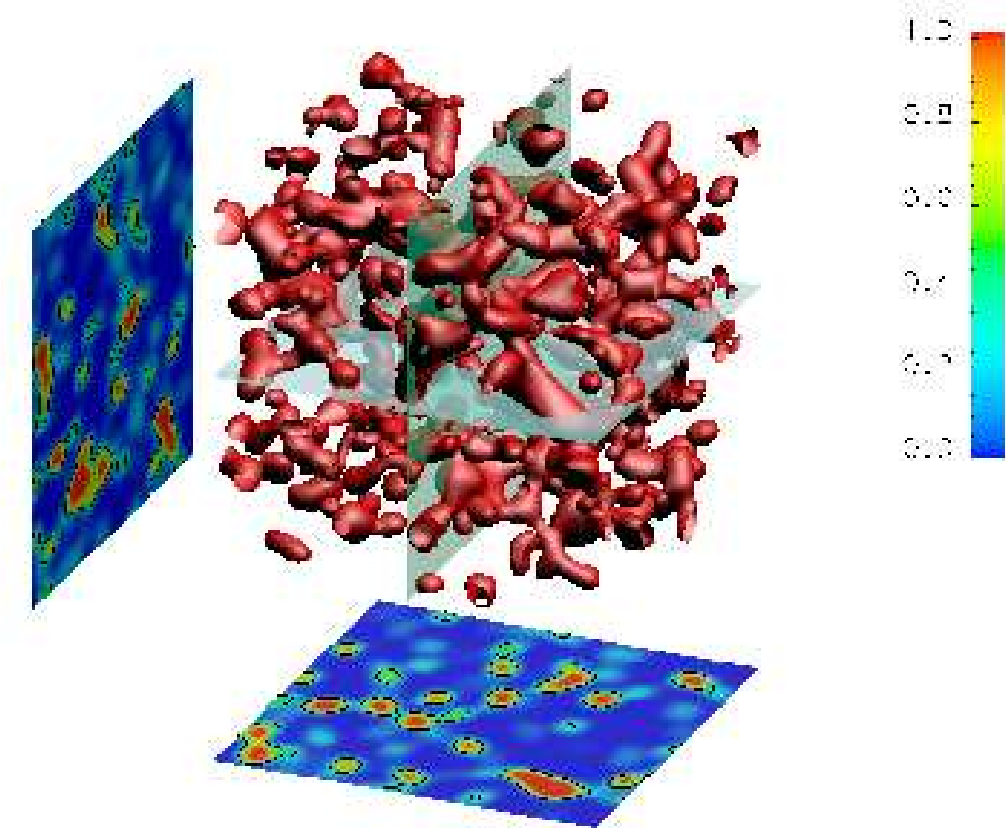


**Figure3.** Transient state of the evolution of the initial state in Figure 2 according to model (3). The initial formation of network-like structures is observed

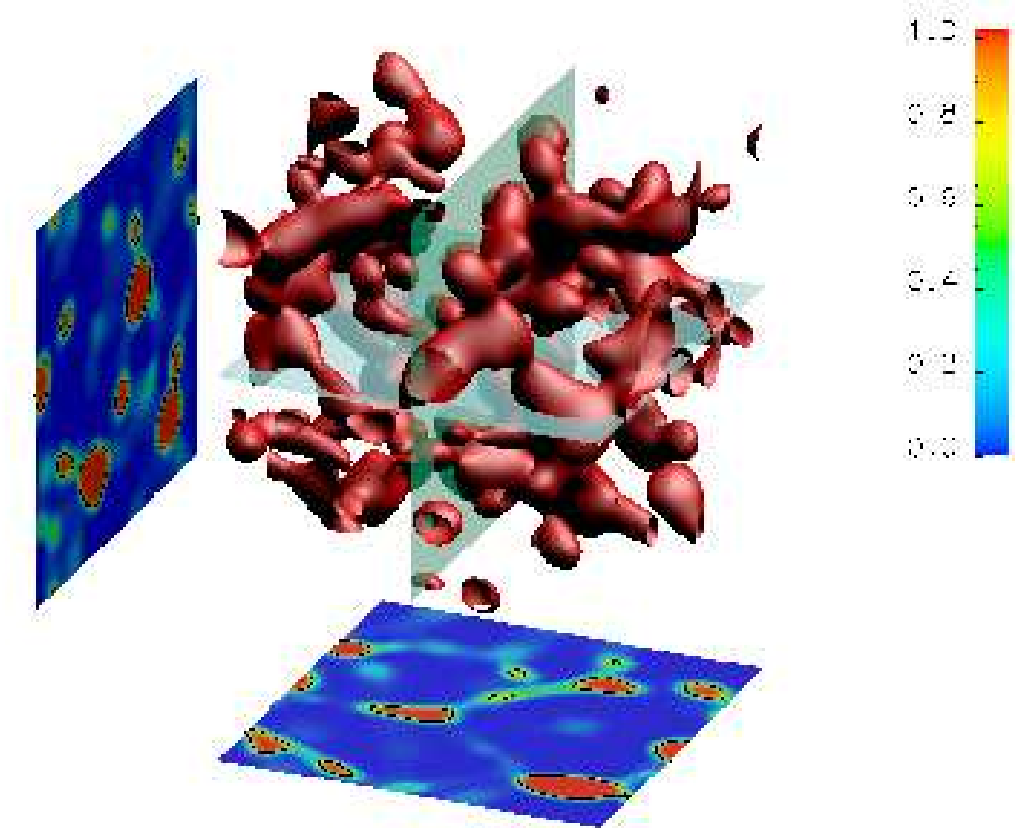


**Figure4.** Stationary state of the evolution of the states in Figures 2 and 3 according to model (3). A well developed network-like structures is observed

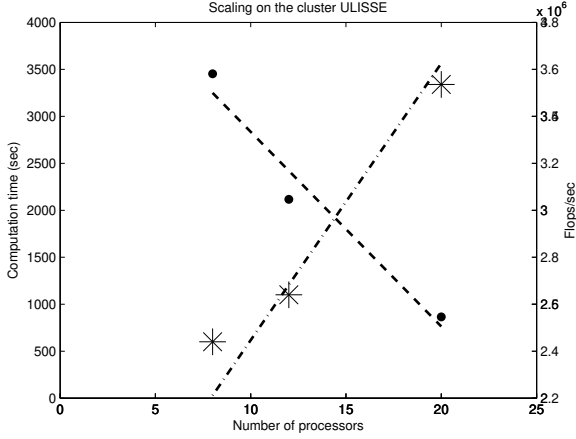


**Figure5.** Scaling of the 3D algorithm on the cluster ULLISSE. The dots represent the execution time (in seconds) and the asterisks the Mflops/sec for our numerical algorithm. The dashed and dash-dot line are their respective linear interpolations

In a neighborhood of the critical point and on a system of finite size  $L$ , the following finite size scaling relations are observed:

$$\Pi(\bar{n}, L) \sim \hat{\Pi}[(\bar{n} - n_c)L^{1/\nu}] \quad (9a)$$

$$P(\bar{n}, L) \sim L^{-\beta/\nu} \hat{P}[(\bar{n} - n_c)L^{1/\nu}] \quad (9b)$$

$$S(\bar{n}, L) \sim L^{\gamma/\nu} \hat{S}[(\bar{n} - n_c)L^{1/\nu}] \quad (9c)$$

Another quantity of interest is the density function  $\rho(r)$  of the percolating cluster for various  $r$ . This function is defined as the mean density of sites belonging to the percolating cluster, enclosed in a circle of radius  $r$  centered at one site belonging to the cluster, and averaged over different centering sites and different realizations of the system. For a fractal object with fractal dimension  $D$ , this should scale as  $\rho(r) \sim r^{D-d}$ . This behavior is expected for percolating clusters at the critical point. It is well known that only two critical exponents are independent, since critical exponents are constrained by scaling laws [21]. To characterize the observed percolative phase transition, extensive numerical simulation of system (3) were performed using lattice sizes  $L = 1, 0.78, 0.62, 0.5\text{mm}$ , with different values of the initial density  $\bar{n}$ . For each point 10 to 15 realizations of the system of size 1mm were computed, depending on the proximity to the critical point.

We thus mapped the continuous density  $n(\mathbf{x})$  to a set of occupied and empty sites by choosing a threshold  $n_0$ . We then measured for each set of realizations:

1. the percolation probability  $\Pi$ ;

2. the fraction of sites belonging to the largest cluster, which for an infinitely large system gives the percolation strength  $P$ ;
3. the mean cluster size  $S$ .
4. the cluster distribution function  $N_s$ .

Figure 6 show examples of percolating and non percolating clusters. Connected clusters are labeled with indices, corresponding to different colors in Figure 6; the largest, percolating clusters is singled out and shown alone.

Using relation (9a), we estimate the position of the critical point  $n_c$  and the value of the critical exponent  $\nu$ . Their values are such that all the data for different box side length and initial density, after rescaling the densities as  $\hat{n} = (\bar{n} - n_c)L^{1/\nu}$ , should lie on the same curve. For fixed  $n_c$  and  $\nu$  we rescale  $\bar{n}$  as before and fit all data with a logistic curve, then compute the difference of the data from this curve. This latter is minimized in the least square fashion to obtain estimates for  $n_c$  and  $\nu$ .

In our case we obtain  $n_c = 2658$  and  $\nu = 0.74$ . While the critical density  $n_c$  depends of the choice of the threshold  $n_0$ , but the critical exponent  $\nu$  is invariant.

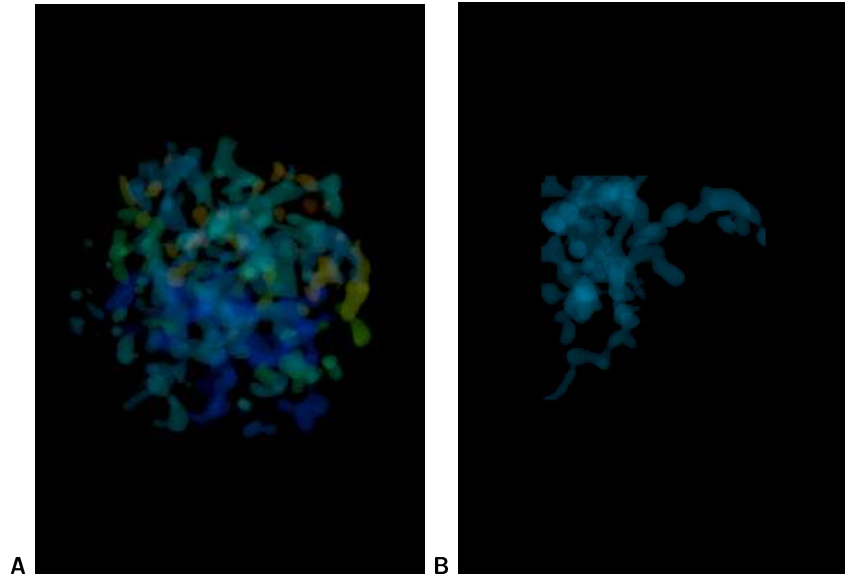


**Figure 6.** Cluster percolation with cell density  $n = 2500 \text{ cells/mm}^3$ . **A:** connected clusters in a realization of model (3). **B:** the largest cluster depicted in A percolates.

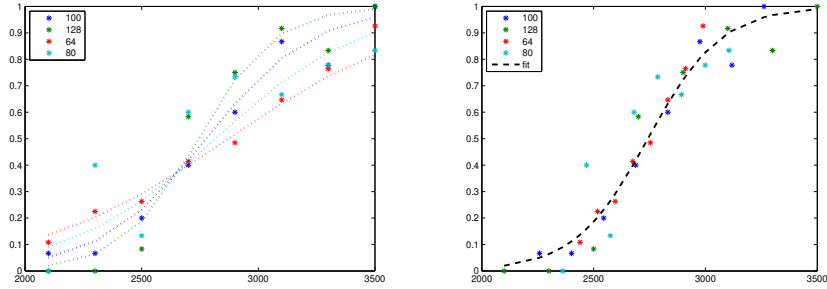


**Figure7.** Percolation probability at varying densities A: B: the curves in A are collapsed according to formula (9a)

## 7 Conclusions

We have exposed preliminary results on the investigation of vascular network formation in a threedimensional setting both from an experimental and a theoretical point of view.

Images of vascular network formation in chick embryo at different stages of development have been obtained by confocal microscopy, showing different stages of development of a vascular network in chick embryo. At an early stage of development one observes typical immature vascular networks formed by vasculogenesis. At subsequent stages one observes initial remodelling, which becomes more evident at later stages, where blood vessels become organized in a mature and hierarchically organized vascular network.

As a computational model we have then consider the natural threedimensional extension of the model proposed in Refs. [7, 19]. Evolution of the computational model starting from initial conditions mimicking the experimentally observed ones produce network-like structures qualitatively similar to those observed in the early stages of in vivo vasculogenesis.

In order to develop a quantitative comparison between experimental data and the theoretical model we have selected a set of observable quantitatis which provide robust quantitative information on the network geometry.

The lesson learned from the study of twodimensional vasculogenesis is that percolative exponents are an interesting set of such observables, so we tested the computation of percolative exponents on simulated obtained network structures.

A quantitative comparison of the geometrical properties of experimental and computational network structure will become possible as soon as an adequate amount of experimental data, allowing proper statistical computation, will be come available.

Other geometrical properties, like the degree of connectivity, that have been previously studied in the twodimensional setting [13, 5] can be also studied in three dimensions.

Our work could in principle present some practical implication. Normal tissue function depends on adequate supply of oxygen through blood vessels. Understanding the mechanisms of formation of blood vessels has become a principal objective of medical research, because it would offer the possibility of testing medical treatments *in silicio*. One can think that the dynamical model (3) can be utilized in the future to design properly vascularized artificial tissues by controlling the vascularization process through appropriate signaling patterns. Moreover, vascular geometry becomes very important in tissue engineering.

Some recent results [18] seem to confirm that a mechanism similar to that studied here could be really working in Nature. It is known that the soluble growth factor VEGF-A exists in several isoforms characterized by different molecular weights and diffusivities. In Ref. [18] it was shown that mouse embryos engineered to express solely an isoform of VEGF-A characterized by larger diffusivity exhibit a specific vessel patterning defect that results in the creation of capillary networks with larger mesh size.

## References

1. A. Abbott. Cell culture: biology's new dimension. *Nature*, 424(6951):870–2, 2003.
2. J. Burgers. *The non linear diffusion equation*. D. Reidel Publ. Co., 1974.
3. P. Carmeliet. Mechanisms of angiogenesis and arteriogenesis. *Nature Medicine*, 6:389–395, 2000.
4. E. Cukierman, R. Pankov, D.R. Stevens, and K.M. Yamada. Taking cell-matrix adhesions to the third dimension. *Science*, 294(5547):1708–12, 2001.
5. S. Di Talia, A Gamba, F. Lamberti, and G. Serini. Role of repulsing factors in vascularization dynamics. *Phys. Rev. E*, 73:041917–1–11, 2006.
6. P. Friedl. Dynamic imaging of the immune system. *Curr Opin Immunol*, 16(4):389–93, 2004.
7. A. Gamba, D. Ambrosi, A. Coniglio, A. de Candia, S. Di Talia, E. Giraudo, G. Serini, L. Preziosi, and F. Bussolino. Percolation, morphogenesis, and Burgers dynamics in blood vessels formation. *Phys. Rev. Lett.*, 90:118101, 2003.
8. A.C. Guyton and J.E. Hall. *Textbook of medical physiology*. W.B. Saunders, St. Louis, 2000.
9. A. Harten. *J. Comp. Phys.*, 493:57, 1983.
10. S. Jin, L. Pareschi, and G. Toscani. *SIAM J. Numer. Anal.*, 35:2405, 1999.
11. S. Jin and Z. Xin. The relaxation schemes for systems of conservation laws in arbitrary space dimension. *Comm. Pure and Appl. Math.*, 48:235–276, 1995.
12. M. Kardar, G. Parisi, and Y.C. Zhang. Dynamical scaling of growing interfaces. *Phys. Rev. Lett.*, 56:889–892, 1986.
13. F. Lamberti, A. Gamba, and B. Montrucchio. Computer-assisted analysis of *in vitro* vasculogenesis and angiogenesis processes. *J. of WSCG*, 12:237–244, 2004.
14. R.J. LeVeque. *Numerical methods for conservation laws*. Birkhauser, Zurich, 1990.
15. B.B. Mandelbrot. *Fractal geometry of nature*. Freeman and Co., San Francisco, 1988.
16. G. Naldi and L. Pareschi. Numerical schemes for hyperbolic systems of conservation laws with stiff diffusive relaxation. *SIAM J. Numer. Anal.*, 37:1246–1270, 2000.
17. Alain Pluen, Paolo A. Netti, Rakesh K. Jain, and David A. Berk. Diffusion of macromolecules in agarose gels: comparison of linear and globular configurations. *Biophysical Journal*, 77:542–552, 1999.

18. C. Ruhrberg, H. Gerhardt, M. Golding, R. Watson, S. Ioannidou, H. Fujisawa, C. Betsholtz, and D.T. Shima. Spatially restricted patterning cues provided by heparin-binding VEGF-A control blood vessel branching morphogenesis. *Gen. Devel.*, 16:2684–2698, 2002.
19. G. Serini, D. Ambrosi, E. Giraudo, A. Gamba, L. Preziosi, and F. Bussolino. Modeling the early stages of vascular network assembly. *EMBO J.*, 22:1771–9, 2003.
20. S.F. Shandarin and Ya.B. Zeldovich. The large-scale structure of the universe: turbulence, intermittency, structures in a self-gravitating medium. *Rev. Mod. Phys.*, 61:185–220, 1989.
21. H.E. Stanley. *Introduction to Phase Transitions and Critical Phenomena*. Oxford University Press, 1987.
22. D. Stauffer and A. Aharony. *Introduction to Percolation Theory*. Taylor & Francis, London, 1994.
23. P.R. Sweeny. *SIAM J. Num. Anal.*, 21:995, 1984.
24. G.B. West, J.H. Brown, and B.J. Enquist. A general model for the origin of allometric scaling laws in biology. *Science*, 276(5309):122–6, 1997.
25. G.B. West, J.H. Brown, and B.J. Enquist. The fourth dimension of life: fractal geometry and allometric scaling of organisms. *Science*, 284(5420):1677–9, 1999.